



# CHORUS

This is the accepted manuscript made available via CHORUS. The article has been published as:

## Nanoscale structure of the magnetic induction at monopole defects in artificial spin-ice lattices

C. Phatak, A. K. Petford-Long, O. Heinonen, M. Tanase, and M. De Graef

Phys. Rev. B **83**, 174431 — Published 18 May 2011

DOI: [10.1103/PhysRevB.83.174431](https://doi.org/10.1103/PhysRevB.83.174431)

# Nanoscale structure of the magnetic induction at monopole defects in artificial spin-ice lattices

C. Phatak,<sup>1,\*</sup> A. K. Petford-Long,<sup>1,2</sup> O. Heinonen,<sup>1,3</sup> M. Tanase,<sup>1,†</sup> and M. De Graef<sup>4</sup>

<sup>1</sup>*Argonne National Laboratory, 9700 S. Cass Avenue, Argonne, IL 60439, USA*

<sup>2</sup>*Dept. of Materials Science and Engineering, Northwestern University, 2220 Campus Drive, Evanston, IL 60208, USA*

<sup>3</sup>*Dept. of Physics and Astronomy, Northwestern University, 2145 Sheridan Rd, Evanston, IL 60208-3112*

<sup>4</sup>*Dept. of Materials Science and Engineering, Carnegie Mellon University,  
5000 Forbes Avenue, Pittsburgh, PA 15213, USA*

Artificially frustrated spin-ice systems are of considerable interest since they simulate the spin frustration and concomitant rich behavior exhibited by atoms on a crystal lattice in naturally occurring spin-ice systems such as pyrochlores. As a result of the magnetic frustration these systems can exhibit “magnetic monopole” type defects, which are an example of an exotic emergent quasiparticle. The local magnetization structure of such monopole defects determines their stability and thus is critical to understanding their behavior. In this contribution, we report on the direct observation at room temperature of the nano-scale magnetic structure of individual magnetic monopoles in an artificially frustrated two-dimensional square spin-ice lattice, using high resolution aberration-corrected Lorentz transmission electron microscopy. By combining the high-resolution microscopy with micromagnetic simulation, we demonstrate how nucleation of defect strings, reminiscent of Dirac strings, connecting monopole defects controls the demagnetization process in these spin-ice lattices.

PACS numbers: 75.75.-c, 75.25.-j, 75.60.Jk

## I. INTRODUCTION

The existence of magnetic monopoles was first predicted by Dirac<sup>1</sup>. They form a part of an exotic class of emergent quasiparticles which fractionalize the underlying quantum numbers<sup>2</sup>. A pair of isolated Dirac monopoles can exist at the ends of a one-dimensional string, now known as a Dirac string, and each end is a singularity in the electromagnetic field. These strings carry the magnetic flux density resulting from the monopoles. Isolated Dirac monopoles have so far never been observed, but certain classes of geometrically frustrated magnetic systems, namely spin ices, have recently been shown to produce defects that are locally isomorphic with Dirac monopoles<sup>3</sup>.

Naturally occurring spin-ice compounds, such as the rare earth pyrochlore oxides  $A_2B_2O_7$ , where  $A$  is a rare earth element and  $B$  a transition metal, contain magnetic ions that reside on a three-dimensional (3-D) lattice of vertex-sharing tetrahedra. The dipolar interaction between nearest neighbor moments favors a “two-in-two-out” magnetization state for each tetrahedron, the so-called “spin-ice rule”, that leaves the tetrahedron with a zero net magnetic charge. Tetrahedra which do not satisfy the “spin-ice rules” carry a net magnetic charge, and can be labeled magnetic monopole defects. That magnetic monopole defects can exist when the spin-ice rule breaks down locally has been reported before<sup>4</sup>. The energetics and dynamics of the low temperature spin-ice pyrochlore system,  $Dy_2Ti_2O_7$ ,<sup>5,6</sup> and  $Ho_2Ti_2O_7$ ,<sup>7</sup> were explained on the basis of magnetic monopole defects using neutron scattering. The existence of ‘magnetic charge’ associated with magnetic monopole defects and their interactions was studied by Bramwell et. al.<sup>8</sup>. There is extensive work going on to understand the low temperature behavior of bulk spin-ice systems and correlate it with the magnetic Coulomb phase or magnetic monopole defect physics. However, these systems exhibit such behavior only at a very low temperature and, as such, direct observation of the individual magnetic moments and interactions between the atoms is difficult.

Artificial 2-D magnetic lattices comprised of hundreds of nanometer-scale magnetic elements provide an interesting alternative for the study of magnetic frustration and related critical phenomena, in particular the formation of magnetic monopole defects and the linking of such defects; the most important reason for studying these systems is the fact that the frustrated state is accessible at room temperature. Using electron beam lithography techniques, one can fabricate periodic arrays of single domain nanomagnets, based on 2-D uniform (or Archimedean) lattices such as the square lattice<sup>9–11</sup> and the Kagome lattice<sup>12–14</sup>. Both lattice types have been shown previously to exhibit frustration and spin-ice effects. A real space observation of the presence of magnetic monopole defects was recently reported in artificially frustrated Kagome spin ice lattices<sup>15,16</sup>. A thermal study of such defects in square lattice was recently reported by Morgan et. al<sup>17</sup>. The realization of monopole type defects on a square lattice with height differences between the islands was also recently reported<sup>18</sup>. However, the detailed magnetic structure of monopole defects has not yet been elucidated, nor how the demagnetization process is affected by the presence and motion of such defects.

Here we investigate the formation of magnetic monopole defects in an artificially frustrated 2-D square lattice using aberration corrected Lorentz transmission electron microscopy (LTEM). The magnetic induction field lines associated with several monopole defects are visualized experimentally. The magnetization of individual magnetic elements and their interactions are mapped out and by combining the advanced imaging techniques with micromagnetic modeling, a coherent picture of the isolated Dirac monopoles and the demagnetization process of the frustrated spin-ice lattice is established.

## II. EXPERIMENTAL METHODS

Aberration-corrected LTEM imaging combined with electron wave phase retrieval provides a high spatial resolution as well as the ability to obtain quantitative magnetic information at a length scale of nanometers, an order of magnitude smaller than what was the norm thus far in uncorrected LTEM<sup>19</sup>. The phase shift of the electrons in the TEM can be retrieved from a through-focus series of Lorentz images using the paraxial *Transport-of-Intensity* approach<sup>20</sup>. The improved signal-to-noise ratio and reduced electron delocalization that come with aberration correction significantly benefit LTEM observations, in the sense that the amount of defocus required to reconstruct the phase shift is significantly reduced. These improvements make possible the direct measurement of the electron magnetic phase shift associated with individual magnetic monopole defects along with the magnetization state of each nanoscale element of the square spin-ice lattice.

For our study, we chose the square lattice, since it is most similar to the pyrochlore vertex-sharing tetrahedral network in that each node is surrounded by four magnetic elements. However, in pyrochlores, all the nearest neighbors to a single magnetic ion are equidistant, whereas all the nearest neighbors of an island in a square lattice are not equidistant. For a given node, there are four possible arrangements of the magnetic moment of the surrounding elements; the four basic node types are shown in Fig. 1(a). The boldface number to the right of each node type indicates its degeneracy. Thus, the spin-ice rule for a square lattice is similar to that for the pyrochlores, with

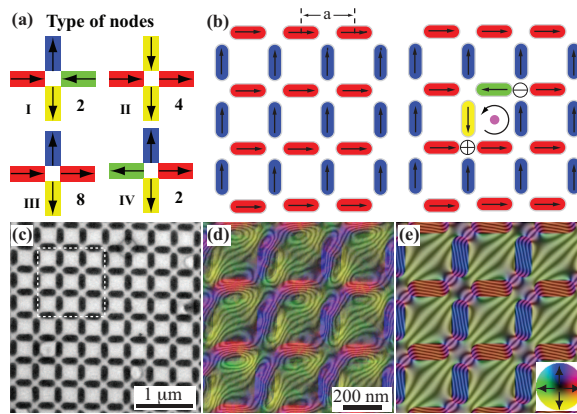


FIG. 1. (Color online) (a) Schematic showing the different types of nodes possible in a square spin-ice lattice; (b) schematic showing the uniformly magnetized square lattice and the generation of a monopole pair ( $\oplus$  &  $\ominus$ ) after flipping the magnetization in two elements and the corresponding vortex state formed indicated by magenta dot and curved arrow; (c) experimental TEM image of the patterned square lattice; (d) magnetic induction color map from the section highlighted in (c) with the cosine of the phase overlaid to show the magnetic interaction between the islands, and (e) similar color induction and phase map computed from micromagnetic simulations.

the most stable configuration corresponding to a two-in-two-out state of type I or type II nodes. Fig. 1(b) shows a schematic of a square lattice with each node set to type II, resulting in a zero net magnetic charge. If the magnetization of two of the elements is reversed, as shown in the second schematic, a net magnetic charge  $Q = \pm q$  (indicated by a  $\oplus$  or  $\ominus$ ) results at either end of the line connecting the reversed elements. By reversing the magnetization of additional neighboring elements, these charges can become separated by a large distance, leading to the formation of “extended dipole”. These defects are similar to Dirac strings in the sense that they both have isolated monopole defects at the ends. However, when multiple such monopole defects exist in the lattice, a unique line connecting any two oppositely charged monopole defects cannot be identified. Along the chain, alternating vortex states, defined by four islands on a square, are formed, as indicated by the curved arrow and the magenta dot in the schematic Fig. 1(b), are formed; on one side of the string, all vortices are clockwise, whereas they are counter-clockwise on the other side. Hence, a monopole defect traveling across the square lattice leaves behind a double row of magnetic vortex states.

The samples were fabricated by electron beam lithography using a JEOL 9300. A single layer of ZEP resist of 100 nm thickness was coated on a Si/SiN substrate, followed by patterning of a square lattice with element shape parameters of  $2L_x = 290$  nm,  $2L_y = 130$  nm, and a lattice spacing of  $a = 390$  nm. Ni<sub>80</sub>Fe<sub>20</sub> (permalloy) film of thickness 20 nm was deposited on a seed layer of Cr (3 nm) using DC magnetron sputtering at 3 mTorr pressure and 50 W power. The pattern was transferred by a lift-off process. This was followed by optical lithography and wet-etching of Si to create electron transparent windows on 3 mm square grids which could be loaded directly into the TEM for observation. The microscopy was performed using the JEOL 2100F TEM equipped with a dedicated Lorentz lens and a spherical aberration corrector. Fig. 1(c) shows a TEM image of such a patterned square lattice. Fig. 1(d) shows the cosine of the magnetic phase map overlaid on the original TEM image of the lattice. The black and white lines are indicative of the magnetic field lines. The colors correspond to the local magnetization direction in the elements and are defined in the color wheel shown in the inset in Fig. 1. The lines from one island interact strongly with those from its neighbors, resulting in a complex interaction pattern. Fig. 1(e) shows the phase map computed from a micromagnetic simulation (see the Appendix for details of the micromagnetic simulations) of the magnetization; there is close agreement between observations and simulations. In particular, it should be noted that the magnetization in each island is not quite uniform but is “S” shaped.

### III. DEMAGNETIZATION OF THE LATTICE

One of the main challenges in artificially frustrated lattices is the fact that it is difficult to achieve a fully demagnetized ground state. In accordance with the spin-ice rule for the square lattice, this would require all the nodes to be in a type I “two-in-two-out” configuration in order to minimize the energy and result in a zero net magnetization for the entire array. Correspondingly this means that the entire lattice would consist of diagonal rows of alternating vortex states (clockwise and counterclockwise). As mentioned earlier, this can be achieved by the motion of monopole defects across the lattice. To study the process of spin-ice lattice demagnetization, our sample was initially uniformly

magnetized, such that all the nodes were of type II and obeyed the spin-ice rule. The magnetization components  $M_x$  and  $M_y$  for an element were assigned the values  $\pm 1$  if they were aligned along the  $\pm x$  or  $\pm y$  axis, respectively. The net magnetization was then computed as  $M = \sqrt{M_x^2 + M_y^2}$ . For the portion of the lattice shown in Fig. 2(a) and (b), the total dimensionless magnetization after saturation was found to be 309.74. The demagnetization cycle was performed by rotating the sample at 1000 rpm in an in-plane field with alternating direction and decreasing magnitude<sup>21</sup>. The field was reduced in steps of 3 Oe and the rate of change of field was set at 11800 Oe/s with the sample held at each field value for 3 seconds.

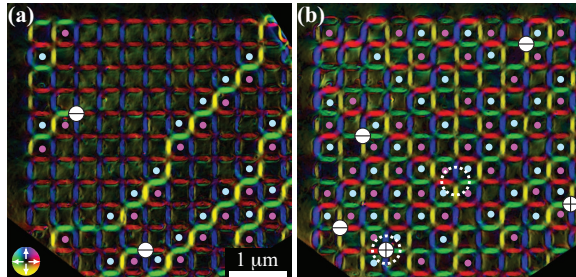


FIG. 2. (Color online) (a) Magnetic induction color map reconstructed after the first demagnetization cycle, showing the formation of defect strings and two magnetic monopole defects with negative charge indicated by  $\ominus$  in the field of view; (b) magnetic induction color map reconstructed after the second demagnetization cycle, showing the presence of many defect strings and 3 monopole defects with negative charge ( $\ominus$ ) and 2 with positive charge ( $\oplus$ ) in the field of view.

The first demagnetization cycle was performed by starting from a field value of 700 Oe, which is above the coercive field of an individual element but below the saturation field of the array, and stopped when the field magnitude was below the coercive field. As a result, the magnetization direction of any individual island in the system could reverse, without magnetic saturation of the total array. The purpose of this cycle was to obtain an intermediate demagnetized state that would allow us to observe the mechanism of demagnetization. Fig. 2(a) shows the magnetic induction map from a corner of the square lattice, reconstructed from the LTEM data. The array edges and corners act as nucleation sites for monopole defects, which then propagate through the rest of the lattice, leaving behind a chain of islands with flipped magnetization similar to Dirac strings (zig-zag lines of alternating yellow/green elements). This observation agrees favorably with micromagnetic simulations indicating that magnetization reversal occurs first along the edges and corners of the lattice. Some chains do not extend all the way to the edges of the lattice but end somewhere inside, leading to the presence of magnetic monopole defects within the lattice. By tracing the defect strings, and accounting for the net magnetic charge at each node, it is found that there are two monopoles of identical sign in the field of view; they are represented by the  $\ominus$  symbols in the image. The net magnetization of this field of view was computed to be 109.4, i.e., a reduction from the saturated value of 309.74, but indicating that the array is only partially demagnetized. The cyan and magenta dots in the image represent clockwise and counter-clockwise vortices, respectively; they are seen to alternate along the yellow-green defect strings.

The second demagnetization cycle was then performed on the same sample with a starting field value of about 1300 Oe, i.e., above the saturation field ( $\sim 900 - 1000$  Oe), with all other conditions identical to those of the first cycle. Fig. 2(b) shows the magnetic induction map from the same corner of the lattice. A greater number of defect strings are present, with alternating vortices adjacent to them. As before, by counting magnetic charges at each node, five magnetic monopole defects are found in the field of view. Three of them have a positive charge indicated by  $\oplus$  symbols, and two are of the opposite magnetic charge indicated by  $\ominus$  symbols. The net magnetization of the field of view was calculated to be 32.4. Thus, after the second demagnetization cycle, the net magnetization is much closer to zero, corresponding to the higher vortex density. This also corresponds to having higher motion of monopole defects through the lattice during the demagnetization process.

From the demagnetization studies, it can be understood that the formation of defect strings and movement of monopole defects is directly responsible for achieving the demagnetized state in the frustrated spin-ice lattice. Fig. 3 shows a plot of the magnetization as a function of the applied field along the diagonal of the square lattice, obtained from micromagnetic (dashed curve) and Monte Carlo simulations (solid curve). The formation of monopole type defects is observed when the applied field goes below the coercive field of 500 Oe, whereupon the magnetization drops rapidly indicating a progression of defect strings through the lattice and flipping of the magnetization of successive islands (Fig. 3(b)). The inset curve shows the monopole density during the magnetization reversal. The slope of the magnetization curve then decreases during which the monopole defects are not able to move freely across the lattice because most of the lattice is transformed except a few islands (Fig. 3(c)). The difference between the two magnetization curves is due to the fact that the Monte Carlo simulation allows only a uniform magnetization while

the magnetization obtained from the micromagnetic simulations can be non-uniform, *e.g.* the ‘‘S’’-state, and also rotate with respect to the applied field.

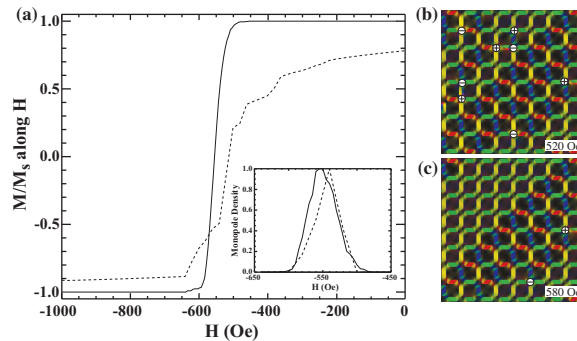


FIG. 3. (Color online) (a) A plot of normalized magnetization and monopole density (inset) as a function of applied field along the diagonal of the square lattice; (b) and (c) show the color coded magnetic induction map from micromagnetic simulations at applied field values of 520 and 580 Oe.

#### IV. MAGNETIC INDUCTION OF A MONOPOLE DEFECT

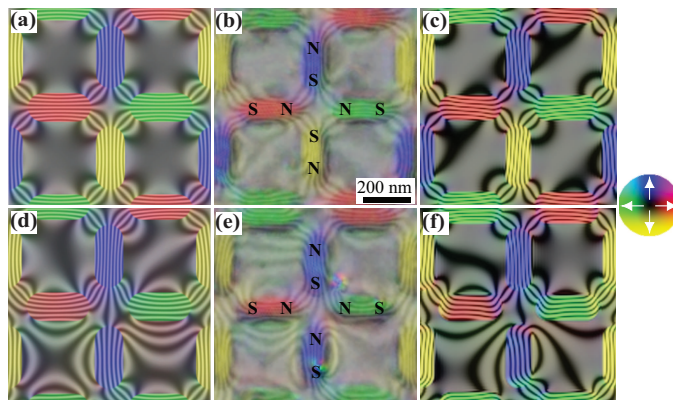


FIG. 4. (Color online) The top row shows phase maps with color coded magnetic induction for a neutral node surrounded by four vortices and the bottom row shows the same for a node with a magnetic monopole defect of positive charge. (a) and (d) show simulated phase maps using the approximation of uniform magnetization for each element, (b) and (e) show the experimentally obtained high resolution phase maps from the two regions circled in Fig. 2(b), and (c) and (f) show simulated phase maps using the micromagnetic simulation data.

The experimental reconstructed phase maps have sufficient spatial resolution to study the magnetic monopole defect up close. Fig. 4(b) and (e) show the two regions indicated by dotted circles in Fig. 2(b); the cosine of the phase map is overlaid onto the magnetization color map. Fig. 4(a) and (d) show simulated phase maps for similar configurations but with uniform element magnetization states, and (c) and (f) show simulated phase maps computed using micromagnetic simulations. In Fig. 4(b), the central node with zero net magnetization is surrounded by four vortices. The magnetization of each end of each island can be assigned an ‘N’ for north pole and an ‘S’ for south pole, as shown in the figure. The field lines clearly extend between pairs of north and south poles, and show the combined symmetry of the underlying lattice and magnetization state. Fig. 4(e), on the other hand, shows the field lines associated with a magnetic monopole defect. Using the north/south analogy, we observe that the field lines from the two horizontal islands bend towards the south pole end of the topmost vertical island. The field lines from the bottom vertical island, however, are repelled by the two nearby north poles, and bend away from the horizontal elements. This pattern of magnetic field lines can be considered to be a finger print for a magnetic monopole defect in a square spin-ice lattice. By comparing the micromagnetic simulations with the high resolution data obtained from LTEM, it can be seen that the high-resolution data is capable of producing fine-structure details down to the nanometer

scale. Conversely, in order to correlate micromagnetic modeling with the experimental data, the modeling has to be performed with sufficiently high resolution to capture and understand all the details observed in the experiments. It should be noted that by comparing (a) with (c) and (d) with (f), the assumption of uniform magnetization in each element does form a good first order approximation for the Monte Carlo simulations.

## V. CONCLUSION

Our work shows that aberration-corrected Lorentz TEM, which has only recently become available, can be used in combination with phase reconstruction to directly visualize the magnetization state of individual magnetic monopole defects in an artificial square spin-ice lattice. Our results were found to agree closely with those predicted from micromagnetic simulations. The presence of defect strings, similar to Dirac strings, separating magnetic monopole defects was clearly observed during the demagnetization process of the frustrated lattice. Furthermore, it was established that the fully demagnetized state which follows the “spin-ice” rule requires the formation of alternating (clockwise and counter-clockwise) vortex states adjacent to a defect string through out the lattice. Further study of the mobility of monopole defects through the lattice will help in achieving such a configuration. The ability to employ aberration-corrected LTEM to study defect strings and monopole defects quantitatively, with high spatial resolution, opens up a wide variety of new possibilities, for instance, the study of the quasi-static behavior of strings and monopole defects in response to different external stimuli, e.g., temperature.

## ACKNOWLEDGMENTS

This work was carried out at Argonne National Laboratory, a US DOE Science Laboratory operated under contract no. DE-AC02-06CH11357 by UChicago Argonne, LLC. The funding for the TEM was provided by the MS&E Division of U.S DOE. We also acknowledge use of the Center for Nanoscale Materials at Argonne National Laboratory. MDG acknowledges DOE’s Office of Basic Energy Sciences for partial financial support (DE-FG02-01ER45893).

- \* cd@anl.gov
- † Currently at: National Institute of Standards and Technology, 100 Bureau Drive, Gaithersburg, MD 20899, USA.
- <sup>1</sup> P. A. M. Dirac, Proc. R. Soc. Lond. A **133**, 60 (1931).
- <sup>2</sup> I. Ryzhkin, Journal of Experimental and Theoretical Physics **101**, 481 (2005).
- <sup>3</sup> M. J. P. Gingras, Science **326**, 375 (2009).
- <sup>4</sup> C. Castelnovo, R. Moessner, and S. L. Sondhi, Nature **451**, 42 (2008).
- <sup>5</sup> D. J. P. Morris, D. A. Tennant, S. A. Grigera, B. Klemke, C. Castelnovo, R. Moessner, C. Czternasty, M. Meissner, K. C. Rule, J. U. Hoffmann, et al., Science **326**, 411 (2009).
- <sup>6</sup> L. D. C. Jaubert and P. C. W. Holdsworth, Nature Physics **5**, 258 (2009).
- <sup>7</sup> T. Fennell, P. P. Deen, A. R. Wildes, K. Schmalzl, D. Prabhakaran, A. T. Boothroyd, R. J. Aldus, D. F. McMorrow, and S. T. Bramwell, Science **326**, 415 (2009).
- <sup>8</sup> S. T. Bramwell, S. R. Giblin, S. Calder, R. Aldus, D. Prabhakaran, and T. Fennell, Nature **461**, 956 (2009).
- <sup>9</sup> R. F. Wang, C. Nisoli, R. S. Freitas, J. Li, W. McConville, B. J. Cooley, M. S. Lund, N. Samarth, C. Leighton, V. H. Crespi, et al., Nature **439**, 303 (2006).
- <sup>10</sup> G. Möller and R. Moessner, Physical Review Letters **96** (2006).
- <sup>11</sup> A. Remhof, A. Schumann, A. Westphalen, H. Zabel, N. Mikuszeit, E. Y. Vedmedenko, T. Last, and U. Kunze, Physical Review B **77** (2008).
- <sup>12</sup> A. Schumann, B. Sothmann, P. Szary, and H. Zabel, Applied Physics Letters **97** (2010).
- <sup>13</sup> Y. Qi, T. Brintlinger, and J. Cumings, Physical Review B **77** (2008).
- <sup>14</sup> A. Westphalen, A. Schumann, A. Remhof, H. Zabel, M. Karolak, B. Baxevanis, E. Y. Vedmedenko, T. Last, U. Kunze, and T. Eimüller, Physical Review B **77** (2008).
- <sup>15</sup> S. Ladak, D. E. Read, G. K. Perkins, L. F. Cohen, and W. R. Branford, Nature Physics **6**, 359 (2010).
- <sup>16</sup> E. Mengotti, L. J. Heyderman, A. F. Rodriguez, F. Nolting, R. V. Hugli, and H. B. Braun, Nature Physics **advance online publication**, (2010), URL <http://dx.doi.org/10.1038/nphys1794>.
- <sup>17</sup> J. P. Morgan, A. Stein, S. Langridge, and C. H. Marrows, Nature Physics **7**, 75 (2011).
- <sup>18</sup> L. A. S. Mol, W. A. Moura-Melo, and A. R. Pereira, Physical Review B **82** (2010).
- <sup>19</sup> S. McVitie and M. Cushley, Ultramicroscopy **106**, 423 (2006).
- <sup>20</sup> D. Paganin and K. A. Nugent, Physical Review Letters **80**, 2586 (1998).
- <sup>21</sup> R. F. Wang, J. Li, W. McConville, C. Nisoli, X. Ke, J. W. Freeland, V. Rose, M. Grimsditch, P. Lammert, V. H. Crespi, et al., Journal of Applied Physics **101** (2007).

## APPENDIX

The micromagnetic simulations were performed using a square mesh with cell size 5 nm, and long-range magnetostatic fields were calculated using discrete Fourier transforms. The materials parameters used were  $M_S = 800$  emu/cm<sup>3</sup>, exchange constant  $A = 1.3 \times 10^{-6}$  erg/cm, and zero anisotropy energy. A system containing a total of 144 stadia was used. Magnetization loops were calculated by first setting the magnetization in all cells in random directions, then applying a field of 1000 Oe along a specific direction [*e.g.*, (110 direction)] and letting the magnetization relax by integrating the Landau-Lifshitz-Gilbert equation

$$\frac{d\hat{\mathbf{m}}}{dt} = -|\gamma_e| \hat{\mathbf{m}} \times \mathbf{H}_{\text{eff}} - |\gamma_e| \frac{\alpha}{1 + \alpha^2} \mathbf{m} \times [\mathbf{m} \times \mathbf{H}_{\text{eff}}], \quad (1)$$

with dimensionless damping  $\alpha = 0.25$ . In Eq. 1,  $\mathbf{m}$  is the local magnetization director,  $|\gamma_e|$  the electron gyromagnetic factor, and  $\mathbf{H}_{\text{eff}}$  the effective field, including external field, magnetostatic field, and exchange interactions. The field was then reduced in magnitude in steps of 20 Oe. The converged magnetization configuration from one field value was given a small random perturbation everywhere and then used as input for the next field value was used as input. To obtain the structures in Fig. 4, a remanent configuration was used as a start template and then the magnetization in 24 stadia about the origin were set in specific directions, after which the magnetization was relaxed in zero applied field.